Interdisciplinary Neurosurgery 19 (2020) 100613

Contents lists available at ScienceDirect

Interdisciplinary Neurosurgery

journal homepage: www.elsevier.com/locate/inat

Technical notes & surgical techniques

Effects of external ventricular drainage decompression of intracranial hypertension on rebleeding of brain aneurysms: A fluid structure interaction study

José Luis Thenier-Villa[a,b,*], Antonio Riveiro Rodríguez[c], Pedro Miguel González-Vargas[d], Rosa María Martínez-Rolán[a], Miguel Gelabert-González[a], Aida Badaoui Fernández[c], Juan Pou[c], Cesáreo Conde Alonso[d]

[a] Department of Surgery, University of Santiago de Compostela, Rúa de San Francisco, s/n, 15782 Santiago de Compostela, Spain
[b] Department of Neurosurgery, University Hospital Arnau de Vilanova, Av. Alcalde Rovira Roure, 80, 25198 Lleida, Spain
[c] Applied Physics Department, EEI, University of Vigo, Lagoas-Marcosende, s/n, Vigo, 36310, Spain
[d] Department of Neurosurgery, University Hospital Complex of Vigo, Estrada de Clara Campoamor, 341, Vigo, 36312, Spain

ARTICLE INFO

Keywords:
Intracranial aneurysm
Rebleeding
Fluid structure interaction
Wall shear stress
Subarachnoid haemorrhage
Hydrocephalus

ABSTRACT

Objectives: The treatment of hydrocephalus using external ventricular drainage (EVD) seems to favour rebleeding of an untreated ruptured aneurysm. FSI studies are valuable to study this environment.
Patients and methods: From December 2014 to December 2017, 61 patients with SAH required EVD due to hydrocephalus, 6 patients had aneurysm rebleeding after the procedure. Two controls for each case was included. DSA studies were used for fluid–structure interaction simulations using two scenarios high ICP (5332 Pa) and low ICP (133 Pa).
Results: Maximum displacement of the wall in HICP was 0.34 mm and 0.26 mm in rebleeding and no rebleeding cases respectively, after EVD (LICP), it was 0.36 mm and 0.27 mm. The difference after implantation of EVD (HICP-LICP) had an average of 0.01567 mm and 0.00683 mm in rebleeding and no rebleeding cases ($p = 0.05$). This measure in low shear areas of the aneurysm was 0.026 and 0.0065 mm in rebleeding and no rebleeding cases ($p = 0.01$).

Effective stress in the HICP was 4.77 MPa and 3.26 MPa in rebleeding and no rebleeding cases ($p = 0.25$). In LICP condition, this measure was 2.28 MPa and 1.42 MPa respectively ($p = 0.33$). TAWSS had no significant differences in the conditions of HICP and LICP.
Conclusion: Changes after EVD placement includes an increase in the wall displacement with greater differences over low shear areas, this had a strong association with rebleeding.

1. Introduction

Subarachnoid hemorrhage (SAH) is an important cause of morbidity and mortality in young patients, representing approximately one third of the potential years of life lost related to stroke [1]. The rupture of a cerebral aneurysm leads to a high mortality and morbidity among the survivors, despite the advances in the medical and surgical management of these patients [2]. An important cause of mortality in these patients is rebleeding of the aneurysm. The incidence of rebleeding of an aneurysm is nearly 23% during the first 72 h, and once this event happens, mortality is about 60% [3]. For this reason, current practice is focused on the repair of the ruptured aneurysm as soon as possible [4].

Retrospective studies have identified several factors related to rebleeding, including the location of the aneurysm, intracerebral and intraventricular hemorrhage, clinical severity, the geometry of the aneurysm, among others [3].

Another common complication in SAH is hydrocephalus. It is estimated that up to 30% of patients with SAH will present acute hydrocephalus at the time of the diagnosis [5]. Acute hydrocephalus is usually treated with a procedure to drain cerebrospinal fluid (CSF) in order to relieve intracranial pressure, this is usually accomplished by the implantation of an external ventricular drainage (EVD), this procedure demonstrated to decrease the morbidity and mortality of these patients [6].

* Corresponding author. Present address: Department of Neurosurgery, University Hospital Arnau de Vilanova, Av. Alcalde Rovira Roure, 80, 25198 Lleida, Spain.
E-mail address: jlthenier.lleida.ics@gencat.cat (J.L. Thenier-Villa).

https://doi.org/10.1016/j.inat.2019.100613
Received 31 July 2019; Received in revised form 13 October 2019; Accepted 21 October 2019

Acute hydrocephalus is a life-threatening condition, and is considered a neurosurgical emergency, in clinical practice some patients are treated with an EVD before the aneurysm is treated. There is controversy in the literature about the increased risk of rebleeding of an intracranial aneurysm after this procedure. A recent *meta*-analysis finds a strong association of these variables, in this study 19% of patients with SAH required EVD, and the incidence of rebleeding was 18.8% in treated patients compared with 6.4% of patients not treated with EVD [7].

Given that evaluating hemodynamics of brain circulation in real conditions is ethically unacceptable, many researchers have focused their efforts in computational fluid dynamics to study this complex disease [8]. More recently, variables such as arterial wall characteristics and patient-specific boundary conditions were possible to include in these simulations through Fluid-Structure Interaction (FSI) methods [9–11]; however, in these works either a simplified geometry of the aneurysm or only one case are used. On the other hand, no analysis before and after the clinical event is analyzed. Then, these prevent from the extraction of general conclusions from these analyses.

In this study, we analyzed hemodynamic and structural changes produced in the aneurysmal wall of patients who underwent EVD surgery and suffered a rebleeding, patients who didn't rebleed after the same procedure were included as a control group. All the patients had a ruptured aneurysm untreated at the time of implantation of the EVD.

2. Materials and methods

2.1. Study population

From December 2014 to December 2017, 219 intracranial aneurysms were diagnosed in University Hospital Complex of Vigo, 61 of these patients required treatment with EVD due to acute hydrocephalus at the time of diagnosis, 6 patients had aneurysm rebleeding after the procedure. For the matched case-control design, 2 controls were chosen for each case. Therefore, 12 patients with similar location and geometric characteristics with no rebleeding after EVD placement were included in the study.

Rebleeding was defined by radiological criteria; for this we considered any increased blood content in a CT scan performed after treatment with an EVD, interpreted by the treating physicians of the patient (including neuroradiologists, neurosurgeons and neurointensivists) as rebleeding. The study corresponds to 18 intracranial aneurysms in 18 patients.

The design of this study was approved by the Research Ethics Committee of Galicia (2018/053). This research was directed by PG-Third Cycle of University of Santiago de Compostela within the institutional agreements of education with University Hospital Complex of Vigo.

2.2. Methodology

2.2.1. Geometry

For the treatment of the geometry, we included the ruptured aneurysm including a parent artery and distal branches. 3D models were obtained from digital subtraction angiography (DSA) InSpace3D sequences (Siemens Medical Solutions, Erlangen, Germany).

Segmentation and generation of STL surfaces was performed using Slicer3D software (Harvard Medical School, Boston, MA, USA) for Mac OS. The surfaces were processed using Meshlab (Visual Computing Lab, Pisa, Italy) and FreeCAD (Juergen Riegel, Werner Mayer, Yorik van Havre, OpenSource, http://freecadweb.org/) to create meshes of ≈100,000 tetrahedral elements with the ANSYS workbench (V19.0, ANSYS Inc., USA). In addition, a layer of 0.1D (D = diameter of the lumen) adjacent to the walls was created.

2.2.2. Fluid model

Ansys Fluent 19.0 software was used to solve the Navier-Stokes and mass conservation equations under the assumption of laminar, incompressible, and non-Newtonian blood flow. The corresponding governing equations are given as:

$$\rho(\vec{u}\,\hat{A}\cdot\nabla\vec{u} + \nabla p - \mu\Delta\vec{u} = 0) \quad (1)$$

$$\nabla\bullet\vec{u} = 0 \quad (2)$$

where $\vec{u}$ and p are the fluid velocity and the pressure, respectively ρ is the density ($\rho = 1060\,kg/m^3$), and μ is the dynamic viscosity of blood. Dynamic viscosity of blood is modeled using a Carreau model [20]. This is given as:

$$\frac{\mu - \mu_\infty}{\mu_0 - \mu_\infty} = (1 + (\Gamma\dot{\gamma}))^{\frac{n-1}{2}} \quad (3)$$

where μ is the effective viscosity depending upon the shear rate $\dot{\gamma}$, μ_0 the viscosity at zero shear rate (μ_0=0.056 Pa·s), μ_∞ the viscosity at infinite shear rate ($\mu_\infty = 0.0035$ Pa·s), Γ the time constant ($\Gamma = 3.313$ s) and n the power law index (n = 0.3568).

2.2.3. Solid model

The arterial wall was assumed as a linearly elastic, isotropic, incompressible, and homogeneous material with a density of $\rho_a = 1000\,kg/m^3$. The elastic modulus and the Poisson ratio were taken as E = 5 MPa and υ = 0.49 respectively. The thickness of the aneurysm was considered t = 0.4 mm [12].

2.2.4. Boundary conditions

Transient pulsatile simulations averaged over several cardiac cycles were performed. Regarding the entrance boundary, the input condition was a sinusoidal profile with a peak speed of 0.5 m/s and a minimum speed of 0.1 m/s. The pulse length was 0.125 s, and the period 0.5 s. The output boundaries were defined as constant pressure outlets, with a pressure close to the mean arterial pressure of a first order brain artery (80 mmHg) [13].

The ends of the arteries were held fixed in the solid model; then, the no displacement condition was assigned them as a structural boundary condition.

2.2.5. Fluid–structure interaction (FSI) model

The following boundary conditions on the FSI interfaces were applied: displacements corresponding to the fluid and solid domain must be compatible, (2) the mechanical actions are in equilibrium in the solid/fluid boundaries, and the fluid obeys the no-slip condition [11].

ANSYS workbench software was used to solve the two-way coupling of the fluid and solid domains. The force data were firstly calculated in Fluent software, and then, transferred to the transient structural analysis module of ANSYS to determine the mesh displacement data. The mesh displacement data were again transferred to the Fluent software. When all the iterations converged, the results were visualized and analysed in ANSYS Results module.

2.2.6. Simulations

The experiment consisted of full-course simulations in two conditions from the same solid. In the first condition (HICP – high intracranial pressure) an external pressure load of 5332 Pa (40 mmHg) was applied on the wall of the whole external geometry excluding inlets and outlets; for the second condition, (LICP - low intracranial pressure) a load pressure of 133 Pa (1 mmHg) was applied. The conditions of inlet velocity, outlets, and thickness of the wall and characteristics of the fluid were the same in both experiments.

2.2.7. Output variables

Wall shear stress (WSS) described as the viscous tension exerted by the blood as it passes through the arterial walls. Low shear areas (LSA),

defined as the area of the aneurysm with a WSS below 10% of the mean parent arterial WSS, were obtained during the simulations [14].

The WSS was also averaged over time. In this case, the time averaged wall shear stress (TAWSS) is determined by integrating the nodal WSS over the cardiac cycle.

Regarding the interaction of the fluid with the dynamic mesh, the displacement of the aneurysmal wall and the Von Mises tension were considered as results.

2.3. Statistics

All the variables of interest produced in the simulations were recorded case by case for the statistical analysis. Given the small sample, the study used a matching method considering controls with similar characteristics of age, gender and location.

We used non-parametric statistical tests to compare groups. A value $p < 0.05$ is assumed to be significant.

3. Results

3.1. Geometry

The dimensions of the height, neck, aspect ratio and clinical variables of the bleeding event are summarized in Table 1.

3.2. Displacement of the wall

There is a positive displacement during the systolic phase in the walls of the aneurysm. The maximum displacement in systole of the wall in the condition of HICP in aneurysms that presented rebleeding was 0.34 mm, in aneurysms that didn't rebleed was 0.26 mm, this same displacement measured after the placement of an EVD (LICP), was 0.36 mm in aneurysms that presented rebleeding and 0.27 mm in aneurysms that did not rebleed.

The difference in wall displacement after implantation of EVD (HICP-LICP) in aneurysms with rebleeding had an average of 0.01567 mm, in aneurysms that did not suffer rebleeding was 0.00683 mm. (Mann Whitney U, $p = 0.05$).

As the main site of rupture is the dome of the aneurysm, and this location usually has a low WSS, even increasing displacements in the neck of the aneurysm could not cause a rupture of the aneurysm. We measured displacement differences in LSA of the aneurysm, (HICP-LICP) measurement was 0.0065 mm in aneurysms with no rebleeding and 0.026 in aneurysms with rebleeding after EVD placement. (Mann Whitney U, $p = 0.01$).

3.3. Von Mises stress

The Von Mises stress distribution and the yield strength allow to predict the failure of the material (rupture of the aneurysm). The effective stress in the HICP condition had an average of 4.77 MPa in aneurysms that rebleed and 3.26 MPa in aneurysms that didn't rebleed (Mann Whitney U, $p = 0.25$). In the LICP condition, the aneurysms that rebleed had an average of 2.28 MPa and the aneurysms that did not rebleed had an average of 1.42 MPa in the Von Mises stress. (Mann Whitney U, $p = 0.33$).

3.4. Wall shear stress

The TAWSS in conditions of HICP had an average of 1.1767 Pa in aneurysms that presented rebleeding and 1.2192 Pa in aneurysms that did not present rebleeding (Mann Whitney U, $p = 0.75$). Under LICP conditions, the mean was 1.1775 Pa in aneurysms that showed rebleeding and 1.2125 Pa in aneurysms that did not rebleed (Mann Whitney U, $p = 0.75$). There are no significant differences in the conditions of HICP and LICP with respect to this variable.

4. Discussion

In this study, we evaluated hemodynamic and structural changes in intracranial aneurysms that presented rebleeding after the implantation of an EVD, matching these cases with patients who didn't rebleed after the same procedure. A summary of the findings is presented in Table 2.

All aneurysms included in this study were initially ruptured aneurysms, the dimensions and the aspect ratio shows no significant differences comparing the rebleeding and no rebleeding group, as is expected from matching methodology. Most studies describe displacement of the wall, Von Mises stress and Wall Shear Stress as the main variables of study, our findings are compatible with previous studies assessing the same variables [15].

4.1. Wall shear stress

The WSS has been described in several studies as a variable related to trophic changes in the wall of the aneurysm. The region of the dome, that is the most common site of rupture, contains areas of low WSS. This hemodynamic condition is linked with mechanobiological phenomena of the endothelium, favoring the degradation of the extracellular matrix, cell death and other inflammatory phenomena leading to a destructive remodeling [16]. It is assumed that a 2 Pa WSS is sufficient to maintain the structure and strength of an aneurysm wall [17].

If we consider the phenomenon of rebleeding after the placement of an EVD, TAWSS does not show significant differences in both conditions, probably because all aneurysms of our study share a common starting event, the rupture of the aneurysm. On the other hand, the scarce effect of geometric changes in relation to the velocity profile usually leads to little significant changes in the aneurysmal WSS after hypertensive effects [18], and the same effect is expected by changing intracranial pressure.

Although TAWSS is similar in both groups, some areas of the aneurysm with low TAWSS may contain areas of trophic changes making them prone to rupture with minimal changes in displacement and effective stress.

4.2. Effective stress and wall displacement

According to MacDonald et al. [19] the rupture stress of an aneurysm varies between 0.73 and 1.91 MPa. In our study, the effective tensions of 2.28 MPa during systole after the placement of the external ventricular drainage, compared with 4.77 MPa prior to the procedure, suggest that intracranial pressure has an important role in the wall effective stress, but the hemostatic effect obtained with intracranial hypertension due to hematoma of hydrocephalus could be more relevant in rebleeding phenomena. Moreover, low effective stress after decompression in aneurysms with no rebleeding, in our study (1.42 MPa)

Table 1
Demographic and geometric distribution grouped by rebleeding status.

	Female:Male	Age (mean, SD)	Height (mean, SD)	Neck (mean, SD)	AR (mean, SD)	WFNS score (mean, SD)
Rebleeding after EVD	4:2	53.33, 13.18	7.36, 1.15	3.4, 0.32	1.93, 0.26	4.66, 0.51
No rebleeding	9:3	51.58, 12.64	6.55, 1.44	3.11, 0.52	1.97, 0.39	4.33, 0.65

Table 2
Hemodynamic and geometric changes after and before EVD implantation grouped by rebleeding status.

	TAWSS HICP Pa (SD)	TAWSS LICP Pa (SD)	Displacement HICP mm (SD)	Displacement LICP mm (SD)	Von Mises HICP MPa (SD)	Von Mises LICP MPa (SD)
Rebleeding	1.1767 (0.30)	1.1775 (0.30)	0.34 (0.28)	0.36 (0.29)	4.77 (2.67)	2.28 (1.47)
No rebleeding	1.2192 (0.34)	1.2125 (0.34)	0.26 (0.10)	0.27 (0.10)	3.26 (1.37)	1.42 (0.94)

could explain why these aneurysms didn't rebleed after ICP decompression.

Although the neck of the aneurysm presents greater effective stress [10], the preferred location of the degenerative changes of the arterial wall contributing to the rupture are located in the aneurysm dome [20,21], increasing the susceptibility to rupture in this site.

Nowadays, establishing the thickness and materials of definite areas in the aneurysm wall for FSI studies is hard to achieve. Some studies analyzed materials obtained from surgery or autopsy, but to date, there is no medical imaging technology with a spatial and temporal resolution enough to determine this information and able to be translated into clinical practice [22]. We must assume that low WSS areas correspond to potential rupture sites [21]. Changes in the effective stress and displacement in these areas would determine the failure of the material easily, causing the rupture of the intracranial aneurysm.

In our study, an increase in the displacement of the wall after the implantation of the EVD was found in patients with rebleeding. After the event of decompression of intracranial hypertension with an EVD, the hot spots of maximum displacement of the aneurysm seems to move to other locations in the aneurysmal geometry (See Figs. 1 and 2). One of the findings in our study suggests that the increase in wall displacement in areas of low WSS are more strongly related to rebleeding than the displacement of the wall over the complete geometry of the aneurysm.

4.3. Intracranial hypertension

The role of elevated intracranial pressure in patients with subarachnoid hemorrhage, either due to acute hydrocephalus or due to the mass effect of a hematoma, is of great importance in the hemodynamic changes. Intracranial hypertension would contribute to the arrest of aneurysmal bleeding [23]. Greater maximum wall displacement in areas of low WSS was found in rebleeding cases compared to control cases, this suggests that the significant reduction of intracranial pressure (up to 40 mmHg or 5332 Pa of difference), after the placement of an EVD would cause a reopening of the initial rupture site, canceling the hemostatic effect of intracranial hypertension, rather than a new rupture of the aneurysmal wall. In our study, we only considered ruptured aneurysms, ICP lowering procedures in patients with unruptured aneurysms behaves differently, so the risk profile in both groups are different also.

5. Limitations

For our study, we included a small and heterogeneous cases of ruptured aneurysms with rebleeding, an event that is infrequent and difficult to capture in clinical practice, matching methods are acceptable under this circumstance but they are far from ideal. The simulations were run based on solids from single radiological explorations obtained after the event of rupture, the significance of the geometric changes after this event and its effect on the validity of the application of these data in ruptured aneurysms is unknown, we didn't found studies who assessed geometric changes after rebleeding.

Data regarding the thickness of the aneurysm and mechanical properties of artery wall, the velocity profile of the inlets, intracranial pressure, and other boundary conditions are not available for most

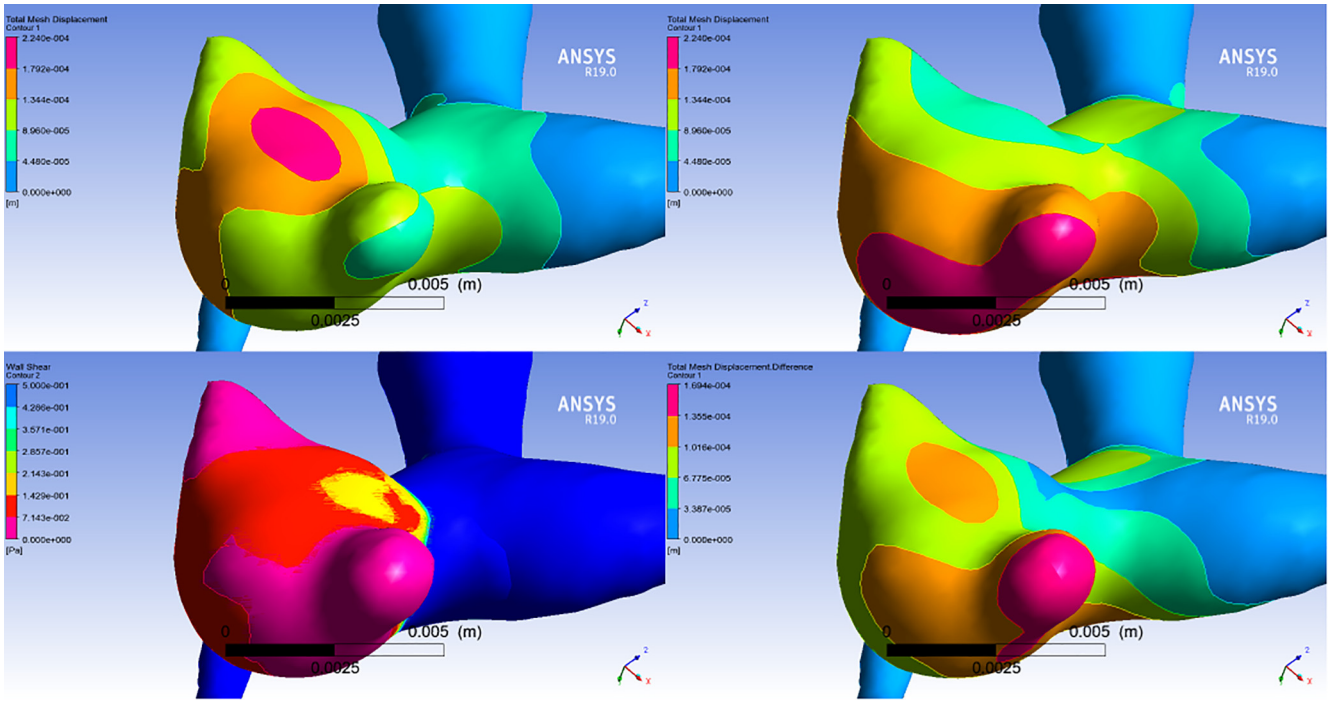

Fig. 1. Wall Displacement and WSS relations in a rebleeding aneurysm case. Upper left: Wall displacement contours before the placement of the EVD. Upper right: Wall displacement contours after the placement of EVD. Lower left: Mid-diastolic WSS showing areas of low stress in two regions of the dome. Lower right: Displacement differences after EVD placement, note congruence with LSA region in an aneurysmal bleb.

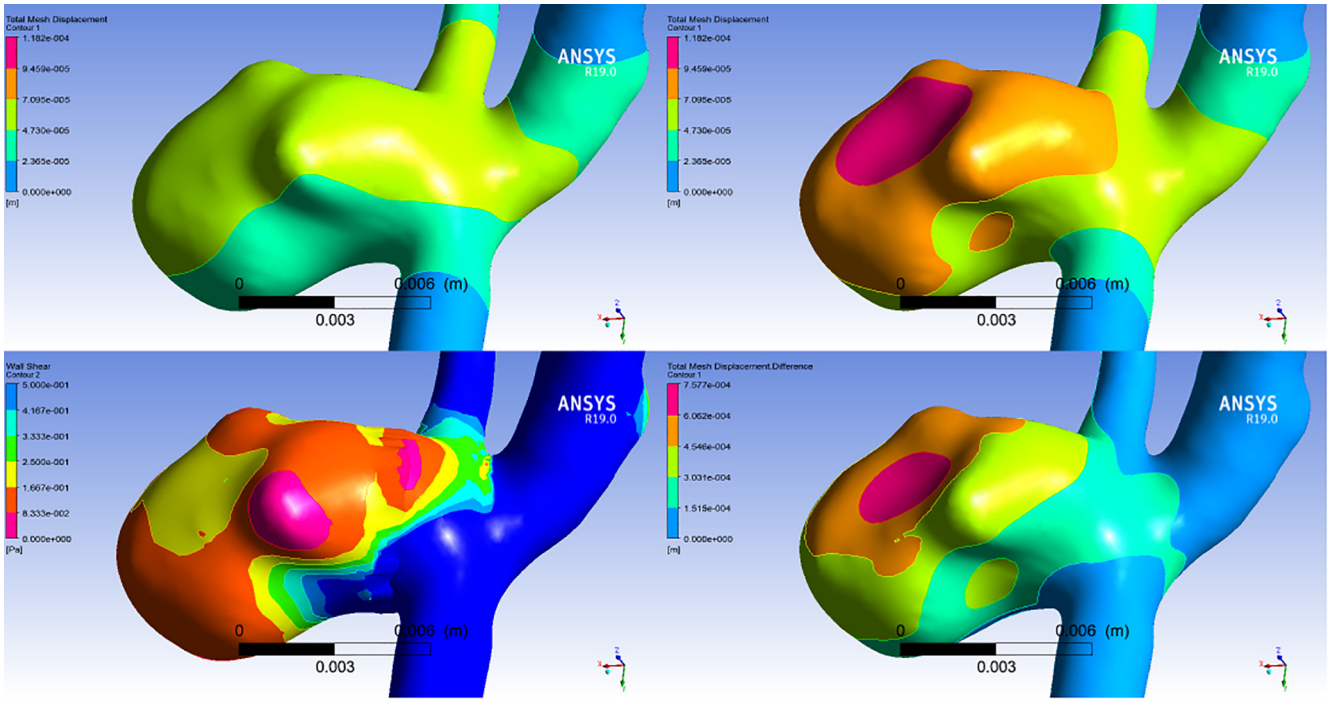

Fig. 2. Wall Displacement and WSS relations in an aneurysm with no rebleeding after EVD. Upper left: Wall displacement contours before the placement of the EVD. Upper right: Wall displacement contours after the placement of EVD. Lower left: Mid-diastolic WSS showing areas of low stress in one region of the dome. Lower right: Displacement differences after EVD placement, note incongruence with LSA region, more displacement was measured in an area distant from LSA.

retrospective studies, we think that certain measures such as homogenization, matching and paired-data analyses could to minimize this problem.

6. Conclusion

Using fluid–structure interaction simulations, structural and hemodynamic changes related to aneurysmal rebleeding after external ventricular drainage placement includes: an increase in the aneurysmal wall displacement over the cardiac cycle. Greater differences in the displacement of the wall over low shear areas of the aneurysm dome have a strong association with rebleeding in our series.

Conflict of interest

None.

Acknowledgements

We gratefully acknowledge our colleagues, medical residents, surgeons, intensivists, nurses and to all the personnel of Complexo Hospitalario Universitario de Vigo, for being always compromised with the care of our most complex patients.

The first author of this study, J. L. Thenier-Villa, gratefully acknowledges Dr. Koichi Hosomi, Dr. Satoru Oshino, Dr. Youichi Saitoh, Dr. Masayuki Hirata, Dr. Manabu Kinoshita, Dr. Hajime Nakamura, Dr. Takeo Nishida, Dr. Naoki Tani, Dr. Hui Ming Khoo, Dr. Haruhiko Kishima and all the personnel of the Department of Neurosurgery, Osaka University Hospital, for their valuable guidance and support.

This work was partially supported by: Xunta de Galicia - Plan I2C Grant Program POS-A/2013/161, ED481B 2016/047-0, ED481D 2017/010).

References

[1] S.C. Johnston, S. Selvin, D.R. Gress, The burden, trends, and demographics of mortality from subarachnoid hemorrhage, Neurology 50 (5) (1998) 1413–1418.
[2] H. Lantigua, S. Ortega-Gutierrez, J.M. Schmidt, et al., Subarachnoid hemorrhage: who dies, and why? Crit Care 19 (2015) 309.
[3] C.C. Larsen, J. Astrup, Rebleeding after aneurysmal subarachnoid hemorrhage: a literature review, World Neurosurg. 79 (2) (2013) 307–312.
[4] G. Grasso, C. Alafaci, R.L. Macdonald, Management of aneurysmal subarachnoid hemorrhage: State of the art and future perspectives, Surg. Neurol. Int. 8 (2017) 11.
[5] J. Lu, N. Ji, Z. Yang, X. Zhao, Prognosis and treatment of acute hydrocephalus following aneurysmal subarachnoid haemorrhage, J Clin. Neurosci. 19 (5) (2012) 669–672.
[6] A.V. Germanwala, J. Huang, R.J. Tamargo, Hydrocephalus after aneurysmal subarachnoid hemorrhage, Neurosurg. Clin. N. Am. 21 (2) (2010) 263–270.
[7] F. Cagnazzo, C. Gambacciani, R. Morganti, P. Perrini, Aneurysm rebleeding after placement of external ventricular drainage: a systematic review and meta-analysis, Acta Neurochir (Wien). 159 (4) (2017) 695–704.
[8] D.M. Sforza, C.M. Putman, J.R. Cebral, Computational fluid dynamics in brain aneurysms, Int. J. Numer. Method Biomed. Eng. 28 (6–7) (2012) 801–808.
[9] Y.G. Stergiou, A.G. Kanaris, A.A. Mouza, S.V. Paras, Fluid-Structure Interaction in Abdominal Aortic Aneurysms: Effect of Haematocrit, Fluids 4 (1) (2019) 11.
[10] A. Valencia, P. Burdiles, M. Ignat, et al., Fluid structural analysis of human cerebral aneurysm using their own wall mechanical properties, Comput. Math. Methods Med. 2013 (2013) 293128.
[11] X. Bai-Nan, W. Fu-Yu, L. Lei, Z. Xiao-Jun, J. Hai-Yue, Hemodynamics model of fluid-solid interaction in internal carotid artery aneurysms, Neurosurg. Rev. 34 (1) (2011) 39–47.
[12] S. Ahmed, I.D. Šutalo, H. Kavnoudias, A. Madan, Numerical investigation of hemodynamics of lateral cerebral aneurysm following coil embolization, Eng. Appl. Computat. Fluid Mech. 5 (3) (2011) 329–340.
[13] P.J. Blanco, L.O. Muller, J.D. Spence, Blood pressure gradients in cerebral arteries: a clue to pathogenesis of cerebral small vessel disease, Stroke Vasc. Neurol. 2 (3) (2017) 108–117.
[14] J. Xiang, S.K. Natarajan, M. Tremmel, et al., Hemodynamic-morphologic discriminants for intracranial aneurysm rupture, Stroke 42 (1) (2011) 144–152.
[15] R. Torii, M. Oshima, T. Kobayashi, K. Takagi, T.E. Tezduyar, Fluid–structure interaction modeling of a patient-specific cerebral aneurysm: influence of structural modeling, Comput. Mech. 43 (1) (2008) 151.
[16] H. Meng, V.M. Tutino, J. Xiang, A. Siddiqui, High WSS or low WSS? Complex interactions of hemodynamics with intracranial aneurysm initiation, growth, and rupture: toward a unifying hypothesis, AJNR Am. J. Neuroradiol. 35 (7) (2014) 1254–1262.
[17] J.D. Humphrey, P.B. Canham, Structure, Mechanical Properties, and Mechanics of Intracranial Saccular Aneurysms, J. Elast. Phys. Sci. Solids 61 (1) (2000) 49–81.
[18] A. Valencia, F. Torres, Effects of hypertension and pressure gradient in a human cerebral aneurysm using fluid structure interaction simulations, J. Mech. Med. Biol. 17 (01) (2017) 1750018.
[19] D.J. MacDonald, H.M. Finlay, P.B. Canham, Directional wall strength in saccular brain aneurysms from polarized light microscopy, Ann. Biomed. Eng. 28 (5) (2000)

533–542.
[20] J. Frosen, R. Tulamo, A. Paetau, et al., Saccular intracranial aneurysm: pathology and mechanisms, Acta Neuropathol. 123 (6) (2012) 773–786.
[21] T. Suzuki, C.J. Stapleton, M.J. Koch, et al., Decreased wall shear stress at high-pressure areas predicts the rupture point in ruptured intracranial aneurysms, J. Neurosurg. 1 (2019).
[22] S. Voß, S. Glaßer, T. Hoffmann, et al., Fluid-structure simulations of a ruptured intracranial aneurysm: constant versus patient-specific wall thickness, Computat. Math. Meth. Med. 2016 (2016) 9854539.
[23] N. Helge, The role of intracranial pressure in the arrest of hemorrhage in patients with ruptured intracranial aneurysm, J. Neurosurg. 39 (2) (1973) 226–234.